INTL JOURNAL OF ELECTRONICS AND TELECOMMUNICATIONS, 2019, VOL. 65, NO.3, PP. 359-365
Manuscript received October 28, 2019; revised August, 2019. DOI: 10.24425/ijet.2019.126322

The Analytical and Artificial Intelligence Methods to Investigate the Effects of Aperture Dimension Ratio on Electrical Shielding Effectiveness

Ibrahim Bahadir Basyigit, Habib Dogan

***Abstract*—This paper presents that the effect of single aperture size of metallic enclosure on electrical shielding effectiveness (ESE) at 0 – 1 GHz frequency range has been investigated by using both Robinson's analytical formulation and artificial neural networks (ANN) methods that are multilayer perceptron (MLP) networks and a radial basis function neural network (RBFNN). All results including measurement have been compared each other in terms of aperture geometry of metallic enclosure. The geometry of single aperture varies from square to rectangular shape while the open area of aperture is fixed. It has been observed that network structure of MLP 3-40-1 in modeling with ANN modeled with fewer neurons in the sense of overlapping of faults and data and modeled accordingly. In contrast, the RBFNN 3-150-1 is the other detection that the network structure is modeled with more neurons and more. It can be seen from the same network-structured MLP and RBFNN that the MLP modeled better. In this paper, the impact of dimension of rectangular aperture on shielding performance by using RBFNN and MLP network model with ANN has been studied, as a novelty.**

***Keywords*—electromagnetic shielding, electromagnetic compatibility, apertures, multilayer perceptron, radial basis function networks**

I. INTRODUCTION

ELECTROMAGNETIC interference has emerged as a major problem with the complexity of electronic circuits. Especially, sensitive electronic equipment may be damaged by this interference. Shielding is one of the major effective methods to reduce the levels of emissions and improve the immunity of electronic equipment. Shielded enclosures and enclosure components usually have apertures for maintenance, cooling and ventilation that they have different pattern and size for control panels, heat dissipation, cables, and other purposes. These apertures decrease the shielding performance and the integrity of the shielded enclosures due to the electromagnetic energy leakage. Also the dielectric mediums have electromagnetic emission excitation characteristics. So, it is important to optimize shielding parameters of enclosures. Shielding effectiveness (SE) performance depends on the frequency, conductivity, permeability and thickness of the sheet enlightened by a plane wave. The enclosure thickness, permittivity, permeability and conductivity are the basic parameters of shielding materials. Most popular and conventional way to determine SE is given as:

$$SE = 20\log\frac{E_r}{E_e} \quad \text{[dB]} \qquad (1)$$

where E_r is the reference electric field magnitude in the absence of an enclosure and E_e is the electric field magnitude in the presence of an enclosure [1]. This is an interconnecting path that causes coupling between electromagnetic energy source and sensitive electronic receiver system.

There are various numerical studies about shielding effectiveness such as Finite Element Methods (FEM) [2], Finite Difference Time Domain (FDTD) [3-6], Transmission Line Matrix (TLM) [7-9], and Moment of Method (MoM) [10-16] and etc. In these numerical methods, it is possible to meet the differences in the solutions for special regions which depend on in spatial, frequency solution, computation time and precise simulation. The major disadvantage of these methods is necessity of more advanced computer resources such as HDD space and RAM etc. Also computations take many hours/days to reach an acceptable solution.

The other method used in this study is about Artificial Neural Networks (ANN) [17-18]. ANN is also a universal approximation method used in electromagnetic researches. But there are not many studies about shielding effectiveness using ANN. A reliability-based design optimization approach for designing electromagnetic shielding structure using neural networks and real-coded genetic algorithm is proposed [19]. A new method is presented for shielded magnetic field level estimation at power frequencies by means of a NN technique which uses experimental data to train and test [20]. There is an attempt to apply ANN in order to estimate the shielded magnetic field for multilayer shielding application [21]. An analytical, a finite element and a NN method are compared with each other to calculate the shielding efficiency of cylindrical ferromagnetic materials with measurement data [22]. ANN, rather than full wave analysis, combines with the

This work was supported by The Department of Scientific Research Projects in Suleyman Demirel University named as 'Investigation the Effect on Total Electromagnetic Emission Distribution of Metallic Enclosure Topology' and in Turkish 'Metalik Kutulama Topolojisinin Toplam Elektromanyetik Emisyon Dağılımına Etkisinin İncelenmesi' [4384-D2-15].

Bahadir Basyigit is with the Department of Electrical and Electronics Engineering, Applied Siciences University, Isparta, TURKEY, (e-mail: bahadirbasyigit@sdu.edu.tr)

Habib Dogan is with Ministry of Environment and Urban, Isparta, TURKEY, (e-mail:habibdogan@gmail.com)

numbered measurements to predict the EM field in the concerned region inside a metallic enclosure [23]. NN is applied to identify various enclosures of apertures which radiate electromagnetic fields. SE of rectangular enclosure has been investigated using the FDTD, software CST and NN method [24].

In this paper, the effect of aperture size of metallic enclosure on ESE has been investigated by using both Robinson's analytical model and ANN methods that are multilayer perceptron (MLP) networks and a radial basis function neural network (RBFNN). All results including measurement have been compared each other in terms of aperture geometry of metallic enclosure. Variation of ESE dependence on aperture length/ width ratio and aperture area in terms of wavelength has been investigated with the assumption of enclosures. The incident plane wave can only have one polarization and direction of travelling which is usually worst case as far as SE is concerned.

Paper is organized as follows: Section 2 exhibits test and measurement set up. Section 3 mentions ANN and its peripherals. Section 4 includes ANN, analytical and measurement results of ESE of metallic enclosure with single aperture. It also contains the comparison of theory and measurement results. Section 5 concludes the manuscript.

II. TEST AND MEASUREMENT SETUP

SE measurements have been performed in a standard anechoic chamber having a dimension of 4×4×8 m. Signal generator operating between DC and 41 GHz and spectrum analyzer have been used as radio equipment. 6 cm long monopole antenna has been used for low frequency band, and ultra-wide band microstrip and standard gain horn antenna have been preferred for high frequency measurements. Both transmitting and receiving antennas have been attached to dielectric rope at 30 cm above the wooden reference table for avoiding any interference. Three different enclosures were selected for ESE measurements. Details of those enclosures are given at Table I.

TABLE I

DIMENSION OF ENCLOSURES AND APERTURES USED IN EXPERIMENT AND SIMULATION

Aperture Case No	*a* (mm)	*b* (mm)	*d* (mm)	*l* (mm)	*w* (mm)	*Area= l×w* (mm^2)
Case 1	800	160	160	75	75	5625
Case 2	800	160	160	150	37.50	5625
Case 3	800	160	160	300	18.75	5625

Measurements have been carried out between 10 MHz - 9 GHz. 10 MHz measurement intervals has been chosen for 10 MHz – 1 GHz low frequency band and 100 MHz for 1 – 9 GHz high frequency band. Each measurement has been repeated 20 times for each frequency and means values have been used to reduce measurement errors. Measurement setup details are shown in Fig.1.

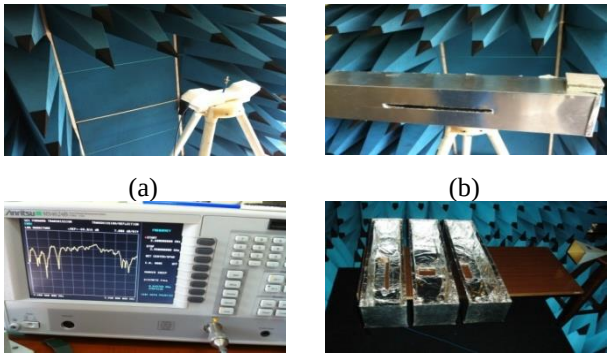

Fig. 1. Measurement Setup: (a) Reference measurement (Absence of enclosure) (b) Measurement with enclosure (Presence of enclosure) (c) Measurements conducted by network analyzer (d) Enclosures having different apertures dimensions

III. MULTILAYER PERCEPTRON

The general structure of multilayer perceptron (MLP) networks is as shown in Fig. 5. MLP is linked to the forward and is usually a structure consisting of an input, an output, and one or more hidden (intermediate) layers [25]. Here, only the most common three-layered MLP, which is based on applications, has been shaped. The input layer allows the input data to be multiplied with the weight values and sent to the hidden layer without using any activation function. Hidden layers send information to the next layer by activating the information with appropriate weights from the input layer. In the end, the output layer processes the information coming from the hidden layers and sets the output values that the network learns against the input data applied from the input layer to the network.

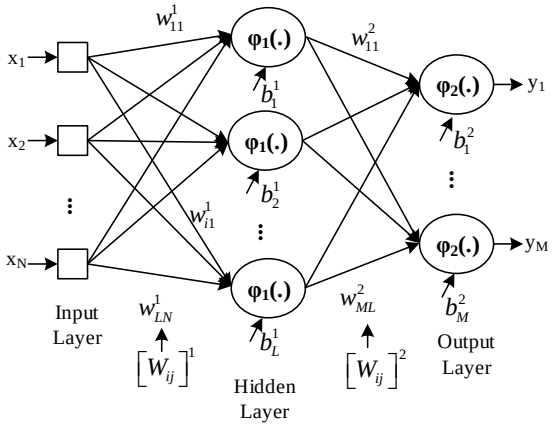

Fig. 2. General structure of MLP

As can be seen in Fig. 2, W_{ij}^{1} weight is the connection between i'th neuron at the first hidden layer and j'th input at the input layer. Also b_i expresses the polarized value of the i'th neuron in the first hidden covert layer. Z_i^1 express the output of the 1st neuron of the 1st hidden layer. In this case, Z_i^1 can be defined as in Eq. (2) and the output of a neuron in the output layer can be also defined as in Eq. (3).

$$z_i^1 = \varphi_1\left(\sum_{k=1}^{N} w_{ik}^1 x_k + b_i^1\right) \quad (2)$$

$$y_i = \varphi_2\left(\sum_{k=1}^{L} w_{ik}^2 z_i^1 + b_i^2\right) \quad (2)$$

MLP network uses a trained learning strategy. Both samples and required outputs obtained by samples are given to network. The network generates a solution space representing the problem space by making generalizations from the samples shown. To learn the network, there is a need of a set of samples called training set. In this set, there are both inputs and outputs to be produced in response to inputs for each sample of the network. MLP consists of two phases, forward and backward calculation. Forward calculation is the calculation phase of the network output. The backward calculation is the phase of changing the weights in order to minimize the error at the output. The universal approximation theory for MLPs was developed [26]. According to this theory, there is a three-layer MLP that provides approximation of the desired accuracy for any non-linear, continuous, multidimensional function. There is no precise information on how many neurons to use in the layers here. The experiential approach that appropriates to the function data for the approximation of the desired accuracy is the shortest solution. It has been experienced that more neurons will be required in the hidden layer of the stage of nonlinear functions and the size of the function. When developing ANN model, the goal is to find the optimal value of the weights matrix as the closest approximation to the input-output relationship of the problem. This is only done by training. In the training data set applied to the network (x_k, d_k) x_k indicates input data and d_k indicates the targeted output values. If k = 1, 2 ... P is taken, then P represents the number of training data pairs. Network performance during training depends on assessing the difference between the network output and the targeted values. So, this difference is also called error and can be defines as in Eq. (4).

$$E = \frac{1}{2}\sum_{i=1}^{P}\sum_{j=1}^{K}(y_{ij} - d_{ij})^2 \quad (4)$$

where the error is defined for the network with K output neurons. As seen in Eq. (4), K value is a function of the inter-layer input, weights and polarization values. By adjusting the weight and polarity (biasing) values and catching the most suitable ones, the error approaches zero and the network performance approaches the best. This is the most fundamental learning algorithm for MLP which has been done for systematic training of ANN [27]. Briefly, it is a method of using the error obtained from the Eq. (4) towards to input (backward) at the output when the input weight and polarization values are updated. The generalized "delta rule" is another name for the back propagation algorithm in the literature. The back propagation algorithm is based on the steepest descent rule, in which weights are shifted in the direction of the negative gradient in the weight space [28].

Generally, weights are updated after each training pattern (training step or training epoch) is applied. This is called on-line training. This approach is often used in situations where different applications are frequently used and the system to be trained is constantly behaving differently. In this method, the network is in continuous learning mode. The cost of this type of learning is very high and is not mostly preferred. Batch training is the most common training mode. Instead of updating the weights at every step of the inputs, it is important to update the weights of the network according to the result values obtained after applying the input training set to the network. Thus, the direction to take the error to the real minimum can be well predicted as it will be moved according to the cumulative result. As a result, we can get rid of the problem of sticking to the local minimum. Derivative based optimization methods are usually used to optimize the objective function generated in ANN applications. These methods find a search direction by taking derivatives of the objective function with respect to the variables. The found direction is towards the smallest point of the objective function. Derivative-based methods can generally be grouped according to their use of first and second derivative knowledge. Some of them are rapid descent, Newton, Gauss-Newton, conjugate gradient, scaled conjugate gradient, Levenberg-Marquardt methods.

IV. Radial Basis Function Neural Networks (RBFNN)

RBFNN performs the mapping process in a similar way to ANN [29]. But the structure and the function of the units are different. RBFNN consists of three layers: input, hidden layers and output layer. The neurons in the hidden layer and output layers are different. Neurons in the hidden layer that use non-linear radial-based activation functions perform local mapping. In other words, using hyper spheres, it divides the pattern space into pieces. The functions are located at the center of the detection regions in feature space. Each property spans the hidden layer neuron containing a space-sensing region, a radial-based function. Here, the artificial neural cells in the hidden layer do not use the weighted shape of the inputs. The outputs of these cells are determined by the distance between ANN inputs and the center of the basic function and the hidden layer processor neuron structure is shown in Fig. 3.

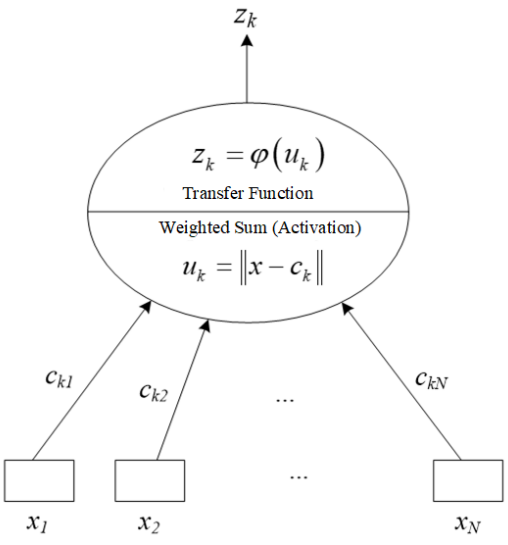

Fig. 3. Processor member of RTFSA hidden layer [28]

There are three components for the radially symmetric hidden layer processor element: the first one is a center vector in the input space. This vector is stored as the weight vector between the input and hidden layers. The second is the distance measure to determine how far an input vector is from the center. Typically, this criterion is taken as the standard Euclidean distance. The last one is an activation function structure that determines the output value of the processor element, which is univariate and receives the distance function output as input. In other words, the output of the hidden layer processor element is only a function of the distance between the center input vectors. This function is ANN structure used in multivariable interpolation approaches. The processor elements in the first layer do not use the weighted shape of the inputs. The last layer of RBFNN constructions is linear and produces a weighted total output from the outputs of the first layer. The general structure of RBFNN can be seen on Fig. 4.

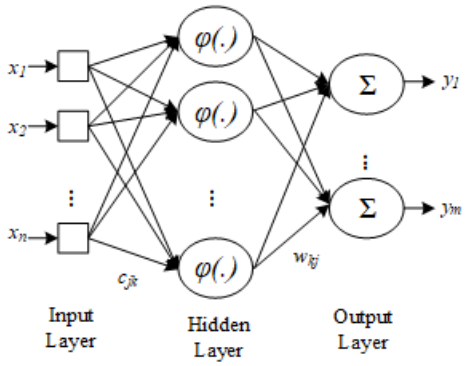

Fig. 4. The general structure of RBFNN

If input vector is close to the center of one of the detection fields, the hidden layer will stimulate the neuron. The input vector is located between the centers of two perception areas. If the region width σ of both perception centers is included, both hidden layer neurons corresponding to this region will be partially stimulated. In the case where input vector is located far from the perception areas, no hidden layer neurons are stimulated and the RBFNN output will be equal to the bias values of the neurons in the output layer. There is local mapping in RBFNN. Only input values near the perception regions can provide for the stimulation of hidden layers. Unlike MLP, global mapping is the opposite, and all inputs form the output value. The choice of radial based functions and their width parameters is important to construct efficient RBFNN. Width does not cover all perception regions, but should not cover all input space with a function. This means that not all hidden layer neurons are stimulated for a single input vector.

Architecture in RBFNN shown in Fig. 5, depending on M hidden layer neurons and N input data (x_i), the net output is calculated by the Eq. (5-7).

$$u_k = \|X - c_k\| = \sqrt{\sum_{j=1}^{N} \left(X_j - c_{ki}\right)^2}, k = 1,2,...,M \tag{5}$$

$$z_k = \varphi\left(\|X - c_{ik}\|, \sigma_{ik}\right) = e^{-\frac{u_k}{\sigma_{ik}^2}} \tag{6}$$

$$y_k = \sum_{j=1}^{M} w_{kj}.z_j, k = 1,2,...,m \tag{7}$$

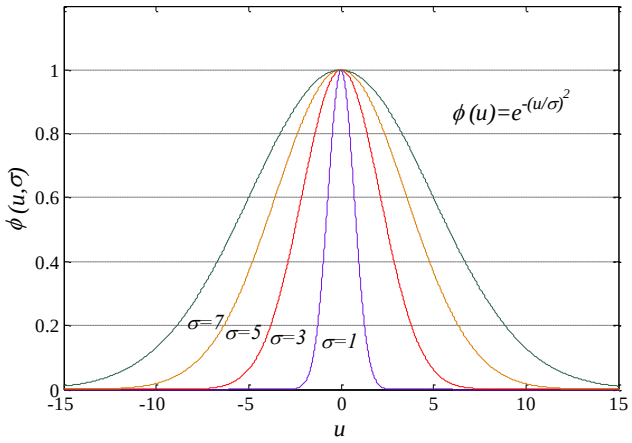

Fig. 5. Gaussian radial basis function

$X=[x_1\ x_2\ \dots\ x_N]^T$ is the multidimensional input vector, c is the center vector that is the same size as the input vector and σ is the standard deviation. In order to train hidden processor elements (pattern units), the center weights of c_k and σ_k must be specified. Like the universal approximation theory for MLP, the universal approximation theory for RBFNN has been developed [31]. According to this theory, a RBFNN network with a sufficient number of hidden layer neurons approximates any nonlinear function with sufficient accuracy. The training parameters for RBFNN are c_{ik}, σ_{ik} and w_{kj} vectors. It is very important to select initial values for the c_{ik} center weight values and classification algorithms (learning without training) are generally preferred. Then the training parameters are updated with gradient-based training algorithms. e_i is the error between target value and RBFNN output. The error function to be minimized depending on the training parameters can be selected as follows in Eq. (8).

$$e_j = \left(d_j - y_j\right)$$
$$E = \frac{1}{2}\sum_{j=1}^{m} e_i^2 \tag{8}$$

where the output function $y = f(x)$ is a function of the hidden layer activation function which is in terms of center weight vector, radial basis function widths (standard deviation), covariance matrix and input vector can be defined with Eq. (9).

$$y = f\left(x\right) = \sum_{j=1}^{M} w_j \varphi\left(\|x - c_j\|\right) = \sum_{j=1}^{M} w_j . e^{-(x-c_j)^T \Sigma_j^{-1} (x-c_j)} \tag{9}$$

Here, Σ_j covariance matrix is the diagonal matrix of σ_j^2 variance values and only the first diagonal has elements when it carries the square and symmetric properties.

V. Results

ANN consisting of forward feed multilayer perception (MLP) type, hidden layer, three inputs and one output is used. The overall ANN block diagram designed for modeling is given in Fig. 6.

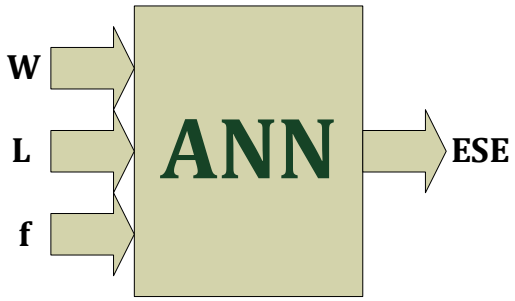

Fig. 6. ANN Model of ESE

The aperture sizes (length and width) indicated in Table 1 are two inputs in network. The frequency of the TE-mode electromagnetic wave propagating from the transmitter is fed as also input parameters. ESE is defined as the output variable. There are 40 neurons in the hidden layer and the hyperbolic tangent is defined as the sigmoidal function activation function. Neurons in the output layer were activated by linear function. The range of values in the input variables is as follows: width and length of aperture Wϵ{75 mm, 150 mm, 300 mm} and Lϵ{18,75 mm, 37,5 mm, 75 mm}, respectively. The frequency (10 MHz, 990 MHz) has been selected by linear division and finally ESE is selected in range of (-23, 72). A total of 297 data samples have been used in the study. The data set has been formed from the measurement results. The study data has been divided into 70% training, 15% validation and 15% test data. In Table II, there are different training algorithms for the training and test data described above. The number of steps that these algorithms achieve in their training and test performance is seen in this table.

Table II

Performance Table for Different Training Algorithms for MLP at the Same Training and Test Data for Analytical (Robinson) Data

Training Algorithm	Minimum Training Error	Number of Steps	Time (sec)
Levenberg-Marquart GM	3.830697e+000	27	1.419
Quasi-Newton GM	1.035030e+001	1000	120.120
Fletcher-Powell	8.426685e+000	37	2.153
Gradient (Steepest) descent	2.014155e+004	6	0.499
Powell-Beale	1.097700e+001	28	1.732
Comparative scaling GM	1.005586e+001	65	3.416

Gradient based Levenberg-Marquardt (LM) back propagation algorithm has been preferred for the smallest test error and fastest training. Also the optimum number of hidden layers and neuron numbers have been selected. The performance function of the forward-feed MLP, average of the squares of the errors (MSE), and number of training steps (training epoch) have been given in Fig. 7. Comparison of ESE results with MLP and analytical (Robinson) model is shown in Fig. 8 and comparison of ESE results with MLP and measurement is illustrated in Fig. 9.

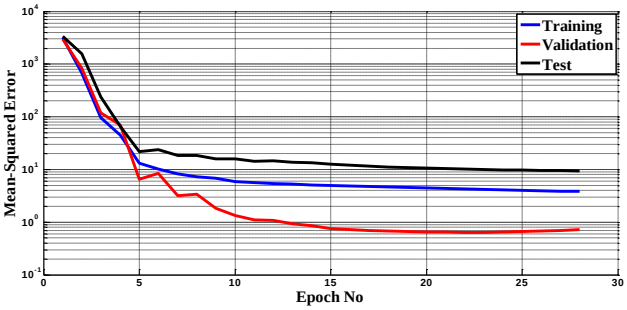

Fig. 7. MLP's LM training algorithm performance of analytical (Robinson) data

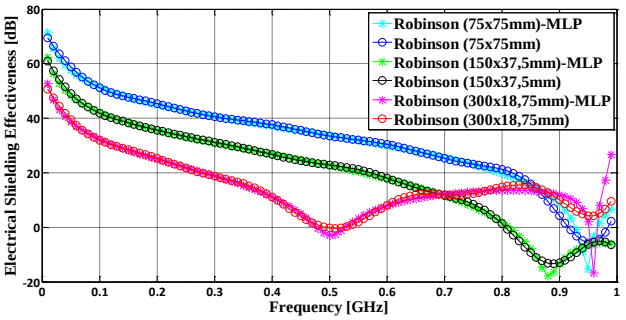

Fig. 8. Comparison of ESE results with MLP modeling of 3-40-1 network and analytical (Robinson) model

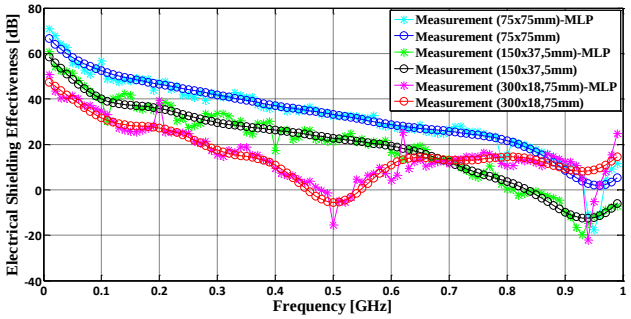

Fig. 9. Comparison of ESE results with MLP modeling of 3-40-1 network and measurement

ANN consisting of RBFNN type, a hidden layer, three inputs and one output has been used. In the hidden layer, 40 and 150 neurons have been tested respectively and the radial-based function has been determined as the activation function. Neurons in the output layer have been activated by linear function. The value range in the input variables is as given above. A total of 297 data sets have been used in the study and the data set has been created separately from the measurement results. The study data has been divided into 50.51% as training and 49.49% as test data.

The root mean square error (RMSE) errors for 40 and 150 step training and tests for MLP and RBFNN are given in Table III. Comparison of ESE results with RBFNN modeling of 3-150-1 network and analytical (Robinson) model is given in Fig. 10 and comparison of ESE results with RBFNN modeling of 3-40-1 network and analytical (Robinson) model is shown in Fig. 11.

TABLE III

RMSE VALUES ACCORDING TO ANN TYPE, NETWORK STRUCTURE, TRAINING AND TESTS

ANN	DATA	NETWORK STRUCTURE	THE ROOT MEAN SQUARE ERROR (RMSE)	
			Robinson	Measurement
MLP	Training	3-40-1	2.0615	2.9549
MLP	Test	3-40-1	3.1931	3.3523
RBFNN	Training	3-40-1	6.0254	5.8893
RBFNN	Test	3-40-1	6.1106	5.8621
RBFNN	Training	3-150-1	0.2731	1.0976
RBFNN	Test	3-150-1	1.1971	2.1136

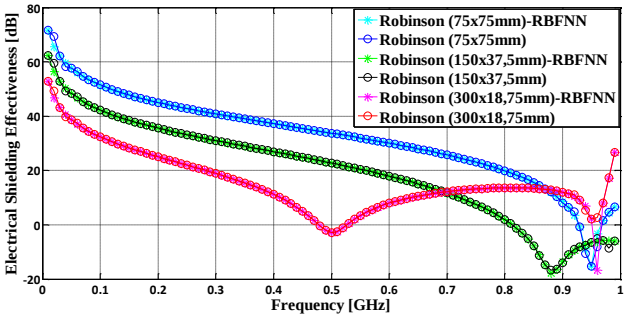

Fig. 10. Comparison of ESE results with RBFNN modeling of 3-150-1 network and analytical (Robinson) mode

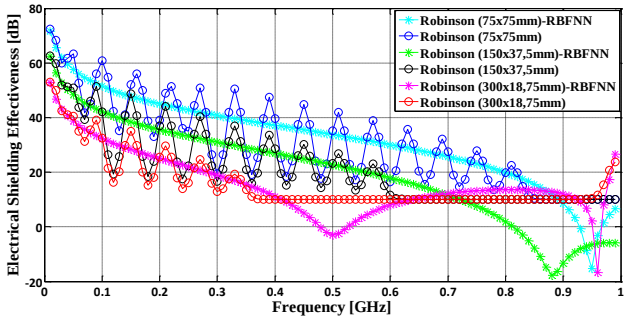

Fig. 11. Comparison of ESE results with RBFNN modeling of 3-40-1 network and analytical (Robinson) model

Comparison of ESE results with RBFNN modeling of 3-150-1 network and measurement is given in Fig. 12 and comparison of ESE results with RBFNN modeling of 3-40-1 network and measurement is shown Fig. 13. When the related tables and figures were examined, it was determined that the network structure of MLP 3-40-1 in modeling with ANN modeled with fewer neurons in the sense of overlapping of faults and data and modeled accordingly. In contrast, the RBFNN 3-150-1 is the other detection that the network structure is modeled with more neurons and more. It can be seen from the same network-structured MLP and RBFNN that the MLP modeled better.

When the analytical and measurement results have been investigated as seen in Fig. 8-13, the total open area of apertures is fixed as 5625 mm2 and ESE changes with the ratio of aperture length/width, the ratios of aperture length/width are 1, 4 and 16 as seen in Table.1. When the aperture has short length with long width, ESE gets higher. When the aperture size is modified from 300 × 18.75 mm to 75×75 mm, ESE gets roughly18-21 dB higher for Fig. 8-13.

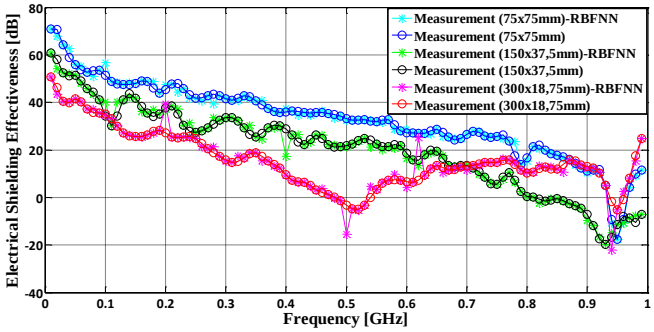

Fig. 12. Comparison of ESE results with RBFNN modeling of 3-150-1 network and measurement

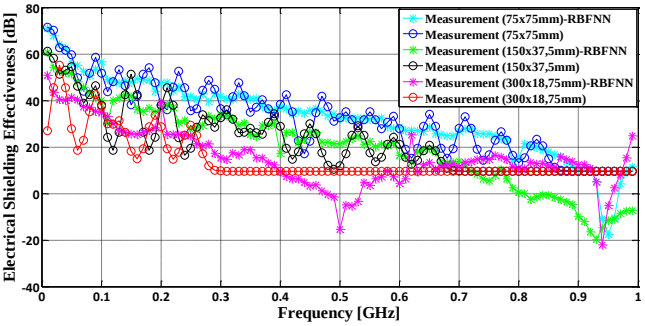

Fig. 13. Comparison of ESE results with RBFNN modeling of 3-40-1 network and measurement

This result can be explained as: parallel polarization of the electric field is horizontal to travelling plane of the wave. So the direction of electric field and the location of aperture length have the same direction, which means that when the aperture length is higher, high amplitude of electric field gets into aperture of enclosure. As a result, ESE changes with polarization of plane wave and the direction of electric field according to the aperture shape (in this situation, it is aperture length).

VI. CONCLUSION

It has been concluded that there is a good agreement between measurement, analytical and ANN results in order to observe the effect of single aperture size of metallic enclosure on ESE at 0 – 1 GHz frequency range. MLP modeling of 3-40-1 network and RFBNN modeling of 3-150-1 network have good performance in the case of comparing with analytical and measurement results.

When the aperture has short length with long width, ESE gets higher. In this situation, designers are required to identify the polarization of incident electric field. For parallel polarization decreasing aperture width and for perpendicular polarization decreasing aperture length are more effective on ESE. First, designers should decrease aperture length for parallel polarization. Second, if the polarization is fixed, they need locate the aperture on enclosure according to the direction of incident angle. Third, producers need locate devices into enclosure according to the aperture width/length ratio. It is important to note that aperture area has no change in these modifications.

REFERENCES

[1] M.P. Robinson, T.M. Benson, C. Christopoulos, J.F. Dawson, M.D. Ganley, A.C. Marvin and et. al. "Analytical formulation for the shielding effectiveness of enclosures with apertures," IEEE Transactions on Electromagnetic Compatibility, Vol. 40, No. 3, pp.240-248, 1998. doi: 10.1109/15.709422

[2] A. Kumar, S. Marwaha, A. Singh, A. Marwaha, "Comparative leakage field analysis of electromagnetic devices using finite element and fuzzy methods," Expert Systems with Applications Vol. 37, No.5, pp.3827-3834. 2010. doi: 10.1016/j.eswa.2009.11.036

[3] H. Azizi,F.T. Belkacem, D. Moussaoui, H. Moulai, A. Bendaoud, M. Bensetti, "Electromagnetic interference from shielding effectiveness of a rectangular enclosure with apertures–circuital approach, FDTD and FIT modeling," Journal of Electromagnetic Waves and Applications, Vol. 28, No.4, 494-514, 2014. doi: 10.1080/09205071.2013.875862

[4] K.F.A. Hussein, "Spatial Filter Housing for Enhancement of the Shielding Effectiveness of Perforated Enclosures with Lossy Internal Coating: Broadband Characterization," International Journal of Antennas and Propagation, Vol. 2013, No. 353647, 2013. doi: 10.1155/2013/353647

[5] C. Jiao, L. Li, X. Cui, H. Li, "Subcell FDTD analysis of shielding effectiveness of a thin-walled enclosure with an aperture," IEEE Transactions on Magnetics Vol. 42, No.4,pp.1075-1078, 2016. doi: 10.1109/TMAG.2006.871638

[6] J.Z. Lei, C. H. Liang, Y. Zhang, "Study on shielding effectiveness of metallic cavities with apertures by combining parallel FDTD method with windowing technique," Progress In Electromagnetics Research, Vol. 74, pp.85-112, 2007. doi: 10.2528/PIER07041905

[7] Q.F. Liu, W.Y. Yin, M.F. Xue, J.F. Mao, Q.H. Liu, "Shielding characterization of metallic enclosures with multiple slots and a thin-wire antenna loaded: Multiple oblique EMP incidences with arbitrary polarizations," IEEE Transactions on Electromagnetic Compatibility Vol. 51, No.2, pp.284-292, 2009. doi: 10.1109/TEMC.2008.2011891

[8] M. Bahadorzadeh,A.L. Neyestanak, A, "Novel and Efficient Technique for Improving Shielding Effectiveness of a Rectangular Enclosure using Optimized Aperture Load," Elektronika ir Elektrotechnika, Vol. 18, No.10, pp.89-92, 2012. doi: 10.5755/j01.eee.18.10.3071

[9] V. Milutinović, T. Cvetković, N. Doncov, B. Milovanović, "Circuital and Numerical Models for Calculation of Shielding Effectiveness of Enclosure with Apertures and Monitoring Dipole Antenna Inside," Radioengineering, Vol. 22, No.4, pp.1249-1257, 2013.

[10] B.L. Nie, P.A. Du, Y.T. Yu, Z. Shi, "Study of the shielding properties of enclosures with apertures at higher frequencies using the transmission-line modeling method," IEEE Transactions on Electromagnetic Compatibility Vo. 53, No. 1,pp.73-81, 2011. doi: 10.1109/TEMC.2010.2047398

[11] R. Araneo, G. Lovat, "An efficient MoM formulation for the evaluation of the shielding effectiveness of rectangular enclosures with thin and thick apertures," IEEE Transactions on Electromagnetic Compatibility, Vol. 50, No.2, pp.294-304, 2008. doi: 10.1109/TEMC.2008.919031

[12] R. Araneo, G. Lovat, "Fast MoM analysis of the shielding effectiveness of rectangular enclosures with apertures, metal plates, and conducting objects," IEEE Transactions on Electromagnetic Compatibility Vol. 51, No.2, pp.274-283, 2009. doi: 10.1109/TEMC. 2008.2010456

[13] P. Dehkhoda, A. Tavakoli, M. Azadifar, "Shielding effectiveness of an enclosure with finite wall thickness and perforated opposing walls at oblique incidence and arbitrary polarization by GMMoM," IEEE Transactions on Electromagnetic Compatibility Vol. 54, No.4, pp.792-805, 2012. doi: 10.1109/TEMC. 2012.2188855

[14] X.C. Nie, N. Yuan, "Accurate modeling of monopole antennas in shielded enclosures with apertures," Progress in Electromagnetics Research Vol. 79, pp.251-262, 2008. doi: 10.2528/PIER07100403

[15] G. Wu, X.G. Zhang, B. Liu, "A hybrid method for predicting the shielding effectiveness of rectangular metallic enclosures with thickness apertures," Journal of Electromagnetic Waves and Applications, Vol. 24, No.8-9, pp.1157-1169, 2012. doi: 10.1163/156939310 791585972

[16] M.F. Xue, W.Y. Yin, Q.F. Liu, J.F. Mao, "Wideband pulse responses of metallic rectangular multistage cascaded enclosures illuminated by an EMP," IEEE Transactions on Electromagnetic Compatibility Vol. 50, No.4, pp.928-939, 2008. doi: 10.1109/TEMC. 2008.927943

[17] Z.B. Zhao, X. Cui, L. Li, B. Zhang, "Analysis of the shielding effectiveness of rectangular enclosure of metal structures with apertures above ground plane," IEEE Transactions on Magnetics, Vol. 41, No.5, pp.1892-1895, 2005. doi: 10.1109/TMAG.2005.846275

[18] V. Devabhaktuni, C.F. Bunting, D. Green, D. Kvale, L. Mareddy, V. Rajamani, "A new ANN-based modeling approach for rapid EMI/EMC analysis of PCB and shielding enclosures," IEEE Transactions on Electromagnetic Compatibility, Vol. 55, No.2, pp.385-394. doi: 10.1109/TEMC.2012.2214223

[19] S. Coco, A. Laudani, F.R. Fulginei, A. Salvini, "A new neural predictor for ELF magnetic field strength," IEEE Transactions on Magnetics, Vol. 50, No.2, pp.69-72, 2014. doi: 10.1109/TMAG.2013.2283022

[20] H. Gargama, S.K. Chaturvedi, A.K. Thakur, "Reliability-based design optimization of electromagnetic shielding structure using neural networks and real-coded genetic algorithm," In Proceedings of the Institution of Mechanical Engineers, Part C: Journal of Mechanical Engineering Science Vol. 228, No.18, pp.3471-3481, 2014. doi: 10.1177/0954406214529556

[21] N. Umurkan, S. Koroglu, O. Kilic, A. Adam, "A neural network based estimation method for magnetic shielding at extremely low frequencies," Expert Systems with Applications Vol. 37, No. 4, pp.3195-3201, 2011. doi:10.1016/j.eswa.2009.09.062

[22] S. Koroglu, N. Umurkan, O. Kilic, F. Attar, "An approach to the calculation of multilayer magnetic shielding using artificial neural network," Simulation Modelling Practice and Theory, Vol. 17, No.7, pp. 1267-1275, Aug. 2009. doi:10.1016/j.simpat.2009.05.001

[23] S. Koroglu, P. Sergeant, N. Umurkan, "Comparison of analytical, finite element and neural network methods to study magnetic shielding," Simulation Modelling Practice and Theory, Vol. 18, No.2, pp.206-216, 2010. doi: 10.1016/j.simpat.2009. 10.007

[24] M. Luo, K. M. Huang, "Prediction of the electromagnetic field in metallic enclosures using artificial neural networks," Progress In Electromagnetics Research, Vol. 116, pp.171-184, Jan. 2011. doi: 10.2528/PIER11031101

[25] D. Sha, V.B. Bajić, "An on-line hybrid learning algorithm for multilayer perceptron in identification problems," Computers & Electrical Engineering Vol. 28, No.6, pp.587-598, 2002.

[26] F.T. Belkacem, M. Bensetti, M. Laour, A. Boutar, M. Djennah, D. Moussaoui and et al, "The analytical, numerical and neural network evaluation versus experimental of electromagnetic shielding effectiveness of a rectangular enclosure with apertures," In Proceedings of the IEEE 9th International Conference on Cybernetic Intelligent Systems (CIS) 2010, Reading, UK:1-6. doi: 10.1109/UKRICIS.2010.5898122

[27] G. Cybenko, "Approximations by super positions of sigmoidal functions, Mathematics of Control, Signals, and Systems, Vol. 2, No.4, pp.303-314, 1989. doi: 10.1007/bf02551274

[28] D.E. Rumelhart, G.E. Hinton, R.J. Williams, "Learning Internal Represantations by Error Propagation. In Parallel Distributed Processing," MIT Press, ICS Report (Datasheet), Technical rept. Mar-Sep. 1988. doi: 10.21236/ada164453

[29] N. P.Thanh, Y. S. Kung, S.C. Chen, H.H. Chou, "Digital hardware implementation of a radial basis function neural network," Computers & Electrical Engineering, Vol. 53, pp.106-121, 2016..

[30] Q.J. Zhang, K.C. Gupta." Neural Networks For RF and Microwave Design," Artech House Publisher, Norwood, MA, 2000.

[31] E. Sağıroğlu, E. Beşdok,M. Erler, Mühendislikte YAPAY ZEKA Uygulamaları - I / Yapay Sinir Ağları. Ufuk Yayınları, Ankara, 2003.